# Ultrafast laser ablation of a multicore polymer optical fiber for multipoint light emission

Research Article Vol. 29, No. 13 / 21 June 2021 / Optics Express 20765
Optics EXPRESS

# Ultrafast laser ablation of a multicore polymer optical fiber for multipoint light emission

HARIKUMAR K. CHANDRASEKHARAN,[1,*] EUNAN P. MCSHANE,[1,2] KEVIN DHALIWAL,[2] ROBERT R. THOMSON,[1,2] AND MICHAEL G. TANNER[1,2]

[1]*Scottish Universities Physics Alliance (SUPA), Institute of Photonics and Quantum Sciences, Heriot-Watt University, Edinburgh, UK*
[2]*Translational Healthcare Technologies Group, Centre for Inflammation Research, Queen's Medical Research Institute, University of Edinburgh, Edinburgh, UK*
[*]*hk47@hw.ac.uk*

**Abstract:** We demonstrate the use of ultrafast laser pulses to precisely ablate the side of polymer multicore optical fibres (MCF) in such a way that light is efficiently coupled out of a set of MCF cores to free space. By individually exciting sets of MCF cores, this flexible "micro-window" technology allows the controllable generation of light sources at multiple independently selectable locations along the MCF. We found that the maximum fraction of light that could be side coupled from the MCF varied between 55% and 73%.



## 1. Introduction

Optical fibres have had profound impact in the biomedical sciences due to their small size, flexibility and low attenuation. Optical fibres generally use an "end-to-end" approach for the transportation of light, in which light coupled into one end of the fibre is transmitted to the other. Some optical fibres, however, can act as distributed light sources that deliver light to the surrounding environment through leakage from the fibre core. Several methods have been implemented to induce side emission from optical fibres, examples of which include the use of micro-bending [1], scattering additives in the fibre [2], asymmetric core-cladding geometries [3], reduced core-cladding refractive indices [4], and diffusive cavities in the fibre core. Distributed light delivery has found numerous applications in areas including photobiomodulation [5], microalgae cultivation [6], laser surgery [7], laser dentistry [8], and antimicrobial applications [9]. Beyond biomedicine, non-medical applications include submersible lighting, decorative lamps, sensing, and textile fabrics.

Recent progress in polymer-based fibre fabrication technology has enabled polymer optical fibres (POFs) that are a low-cost alternative to silica-based fibres providing side emission in many photonic applications. However, in many technical applications, the exponential decay of side-emission light intensity along the POF is not ideal. Overcoming this challenge using light sources at both ends of the POF, or by using an end reflector is not always technically feasible or cost effective. Also, the output coupling efficiency of the side emitting fibres is often low, preventing their use in sensing and imaging applications. To overcome these challenges, several techniques have been demonstrated to create multipoint side-firing waveguides and optical fibres [10–16] to achieve light emission at desired locations. Similar to side-emitting fibre, the side-firing configuration allows the lateral emission of light (relative to the fibre axis), but at discrete locations along the fibre. The aforementioned fabrication techniques used to create side-firing waveguides facilitate controlled side-launching of light but are generally complex, costly, and time consuming to perform. As an alternative method, the precision and feasibility of

#424494 https://doi.org/10.1364/OE.424494
Journal © 2021 Received 11 Mar 2021; revised 24 May 2021; accepted 26 May 2021; published 17 Jun 2021

Optics EXPRESS

ultrafast laser micromachining [17] has been shown to enable the fabrication of micro-windows in glass and plastic optical fibres [18–22]. In comparison to machining using longer laser pulses, femtosecond (fs) laser pulses facilitate more precise and controllable ablation of material [23]. The key motivation for using fs-micromachining is that it is possible to accurately control the geometry of the micro-ablated window structures during manufacturing so that the desired side-emission profile can be obtained.

We present the fabrication of side-emitting micro-windows on a multicore poly-methyl-methacrylate (PMMA) fibre at discrete locations along the fibre length using fs-laser micro-ablation of chosen cores. We demonstrate the ability to control light emission with high precision through control of proximal end coupling of the light, allowing selective or serial illumination from each ablated location along the fibre length. We also demonstrate the ability to control the light emission profile to some degree by further adjusting the proximal coupling.

## 2. Materials and methods

### 2.1. Femtosecond laser micromachining of multicore fibre

Linearly polarised light from a femtosecond laser with central wavelength 1030 nm (Menlo systems) was used to ablatively remove material from selected regions of two PMMA MCFs (MBL-1500 and MBI-1500, Asahi Kasei Co.). The laser operates at a pulse repetition rate of 500 kHz, and the average power of the laser beam on the MCFs was set to 270 mW. The pulse duration at the full width at half-maximum was measured to be ~360 fs, with a peak power of 1.5 MW. Figure 1 illustrates the fabrication set up used to ablate the POFs.

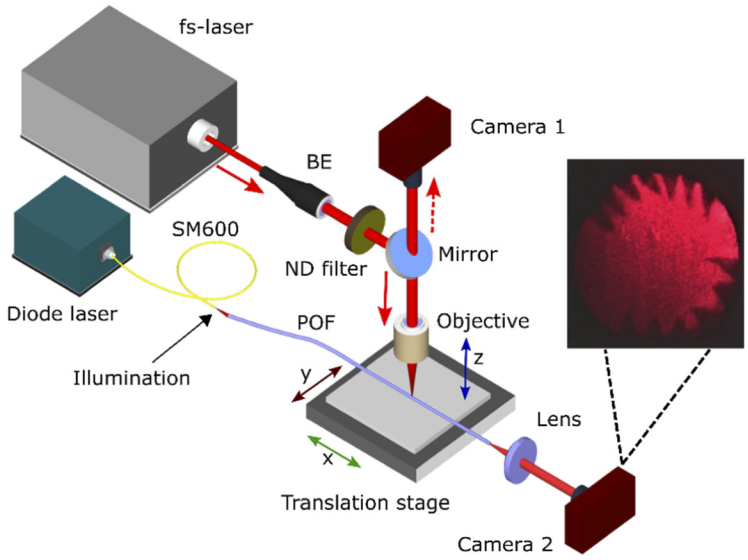


**Fig. 1.** fs-micromachining setup used to create micro-ablated regions at discrete locations along the fibre length. The inset image shows the distal end profile of the POF following the fs-processing. The distal end is imaged during the machining process to ensure the desired ablation profile is obtained.

The laser ablation process is performed by attaching a section of a 1.5 m long PMMA fibre to a high precision computer controllable 3-dimensional (3D) crossed roller translation stage (Aerotech), facilitating the precise positioning of the fibre in all three dimensions. The laser beam is expanded using a beam expander (BE) and guided through a variable neutral density (ND) filter to adjust the laser power delivered to the fabrication system. The ultrafast pulses

Optics EXPRESS

were then focussed tightly on the POF with an aspheric lens with an NA = 0.4. Using this lens, the peak intensity is estimated to be ~$0.7\times10^{14}$ W/cm$^2$. The latter is easily sufficient to induce nonlinear absorption of the laser light [24,25]. This energy deposition results in rapid heating of the exposed material, a phase transformation and ablation of selected regions in the POF. The fs-ablation process can lead to defects in the ablated region such as the formation of a recast layer and formation of a heat affected zone. For controlled alignment of the laser beam to the fibre, a CMOS camera (Camera 1) is used as shown in the experimental layout.

To monitor the fibre ablation process in-situ, the proximal end of the fibre was flood illuminated with a fibre-coupled diode laser (emission wavelength 635 nm). With the opposite end of the fibre imaged onto a CMOS camera (Camera 2), the effect of the fibre ablation on the light transmission can be observed in real-time and thus controlled, Fig. 1. The ablation depth is controlled by moving the POF (translation stage) along the z-axis in Fig. 1. By positioning the fibre on the translation stage and using point-by-point exposure to fs-pulses, a relatively large portion of the MCF is removed, leading to the formation of micron features in the side of the POF with high lateral and axial accuracy. An electronic shutter is used for the laser exposure control (not shown), which precisely initiates and terminates the exposure of the POF to the laser.

Using our fabrication system, two multipoint emission fibres were fabricated using two different fibres – Fibre A and Fibre B. Fibre A exhibited a diameter of 1.5 mm and consisted of 13,000 individual cores. Each core has a diameter of ~12 µm and numerical aperture (NA) of 0.5, meaning it supports ~146 spatial modes at 780 nm. Fibre B exhibited a diameter of 1.5 mm and consisted of 7,400 individual cores. Each core has a diameter of ~16 µm and an NA of 0.5, which supports ~259 spatial modes at 780 nm. As the fibres are based on PMMA, light attenuation within the fibre is relatively high due to the absorption and scattering characteristics of the material. The different loss mechanisms in PMMA fibres are studied extensively elsewhere [26–28] for further reference. The propagation losses of Fibre A and Fibre B at 780 nm were found to be 1.8 dB/m and 1 dB/m respectively, using the fibre cutback method.

12 micro-windows were machined along Fibre A with pitch 20 mm, and 91 micro-windows were fabricated along Fibre B with pitch 10 mm. Once the targeted location on the POF is optimized by moving the stages, the process time for forming a micro-window depends upon the desired size of the structure. The ablation process is performed using a pause-exposure method in which a stepwise transition (step size 50 µm) of the stage is carried out in the z-direction. For each of the transitions (steps), the stages were paused for ~10 seconds, allowing the ablation of the cores from the focussed region, monitored using Camera 2 in Fig. 1. Once the desired depth (size) of the micro-window was obtained, the laser is blocked using the electronic shutter. For an ablation of 200 µm depth 4 steps are required, totalling 40 s, followed by translation to the next location (velocity, 5 mm/s). This results in 40 s exposure for an individual window, therefore 8 minutes total exposure for the 12 points of Fibre A. However, a significantly shorter exposure could be optimised, a cautious approach has been taken here.

As the translation limit of the stages is 100 mm in the x- and y-axis, the fibre was detached from the platform and reinserted to allow fabrication of all 12 micro-windows on Fibre A which span a total length of 220 mm along the fibre (pitch 20 mm), and 91 micro-windows on Fibre B which span 900 mm (pitch 10 mm). This large translation was carried out manually and during each reinsertion the fibre was rotated in order to create micro-windows at different locations around the circumference of the fibre, hence targeting different cores which then allow light to be emitted independently at each micro-window. To optimise the position of individual machined windows and to move between windows, the translation of the stages in the three dimensions was performed in a stepwise manner.

The inset image in Fig. 1 shows the distal end profile of Fibre A after machining to create the 12 micro-windows (note that there are 13 micro-windows in the image, the first micro-window was used for alignment purposes) with the shadows of the machined V-grooves appearing like

Optics EXPRESS

structures on the end facet when the proximal end is flood illuminated. The conical geometries of the micro-windows are clearly visible throughout machining, providing information about the axial position of the focused laser spot with respect to the cylindrical fibre surface during the ablation. It should be noted that each of these V-groove like structures in the inset image is a micro-window formed by the laser exposure and are 20 mm apart along the fibre axis. In the future, a fully automated computer-controlled fabrication system could utilise automated rotational and larger translation stages.

## 2.2. Optical properties of micro-windows

### 2.2.1. Selective micro-window coupling

Fibre A was selected for the optical characterisation of the micro-windows. Results shown in all the figures in the paper (figures in Section 2.2) are from Fibre A. Fibre B is used to demonstrate the capability of our fabrication system to generate many micro-windows in a single fibre. The experimental setup used to characterise the emission profile and fraction of light emitted from the machined micro-windows within the modified fibre is presented in Fig. 2(a). Light from a 780 nm continuous wave laser was coupled into a single mode fibre (SMF) (SM600) with the input end connectorised and the bare output butt-coupled to the polished input end of the POF. The POF was held straight using two custom made fibre mounts, and light was delivered to each micro-window serially by moving the SMF at the proximal end of the POF using a microflexure x-y-z stage. A lensed CCD camera (DCU224C-BG, Thorlabs) was used to image the entire section of the POF containing the laser modified micro-windows with a field of view of ~25 cm × 25 cm (dotted lines).

Light emission from the selected micro-window was optimised by maximising the light intensity observed with the CCD camera as shown in Fig. 2(a). Once the emission is optimised for a specific micro-window, a power meter (PM2) (Thorlabs S121C photodetector (PD2)) was used to measure the output power at the distal end of the POF. This system allows us to optimize the light emission from each micro-window by adjusting the proximal end light coupling in real time. The CCD images of the POF with 12 micro-windows obtained by proximal end white light flood illumination are shown in Fig. 2(b), and four side-emitting micro-windows along the fibre after emission optimisation (selection by butt-coupling) using 780 nm laser light are shown in Figs. 2(c)–2(f). The movie 'Visualization 1' shows the selection of the 91 successive micro-windows in Fibre B in an automated manner.

### 2.2.2. Micro-window radial emission

An initial investigation of the light emission distribution around the circumference of the fibre at four micro-windows was performed. For this, the laser power was measured perpendicular to the fibre axis, in line with the micro-windows. As shown in Fig. 2(a), a power meter (PM1) with photodetector (Thorlabs S121C detector (PD1)) mounted at a distance 20 mm from the fibre on a rotational mount was used to perform the measurements. The mount can be rotated and moved along the various micro-windows without disturbing the fibre.

As the cores in the MCF are closely packed (Fig. 2(g)), the ultrafast laser pulses melt and ablate a group of cores in the POF depending upon the ablation parameters. Figures 2(h) and 2(i) present micrographs of micro-windows when viewed along the z-axis (h) and along the y-axis (i) in Fig. 1. Figure 2(j) presents a cross-sectional image viewed along the x-axis, showing the conical shaped micro-window, with a depth of ~200 µm. To obtain this image, a fibre scoring technique was used in which a small cut is made at the opposite side of the micro-window and the fibre is cleaved by flexing the cut region. The geometry of the micro-structure is clearly visible in the cross-sectional view, along with the heat affected region and the deformed fibre cores surrounding the window, which is presumably the result of localised thermal effects. In future,

Optics EXPRESS

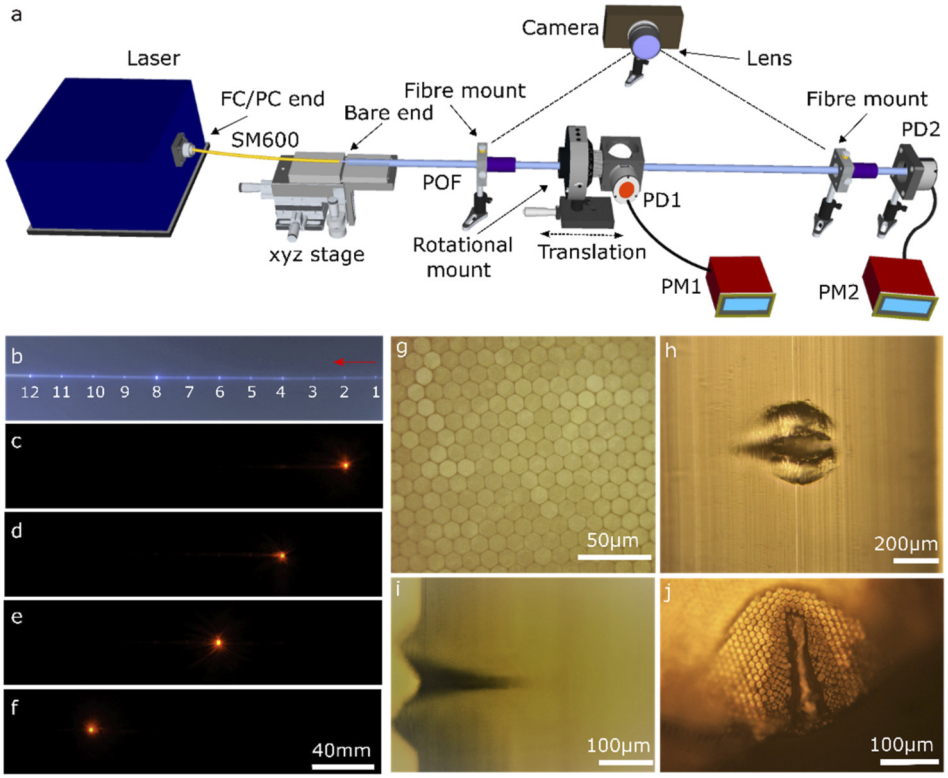


**Fig. 2.** (a) Experimental setup for micro-window characterisation. (b) CCD image of Fibre A with 12 micro-windows under white light flood illumination at the proximal end, ~ 25 cm horizontal field of view. The red arrow indicates the direction of light propagation. (c-f) CCD images showing the distinct light emission from four micro-windows (2, 4, 6 & 10 respectively) under different input coupling conditions. Same scale in b, c, d, e, and f. (g) Micrograph of the fibre facet. (h-j) Micrographs of micro-windows; top view (h), side view (i) and cross-sectional view (j). See the movie Visualization 1 for automated selection of 91 emission points in Fibre B.

the formation of a crater around the surface, and the associated recast layer formation, may be avoided if desired by adopting a water-assisted femtosecond micro-machining approach [21].

The light emission profile and light exit angle from a micro-window strongly depends upon the shape of the ablated crater which can be explained by total internal reflection (TIR). Light incident upon the angled surface of the micro-window reflects from the window when the incident angle exceeds the TIR angle. A simulation model [29] demonstrates that the light incident angle and the geometry of the side-firing window can have a profound effect on the interaction of light with the micro-window, and hence the light emission profile from the micro-windows. The simulation shows the effect of a triangular defect in the fibre core, with a core refractive index of 1.5. Figures 3(a)–3(c) show three situations of (a) side-reflecting, (b) forward refracting and (c) back reflecting light from the micro-window depending on the window's geometry and the incident angle of the light rays. This demonstrates the sensitivity of emission to ablation profile in two dimensions. While the radial dependence is not included in this two-dimensional simulation, it is clear that similar effects would be expected. Particularly in the case presented here, with complex micro-window geometry and coupling to the window coming from a small set of cores

Optics EXPRESS

not necessarily central to the ablated cone, radial emission is expected to have a complex profile so is studied experimentally.

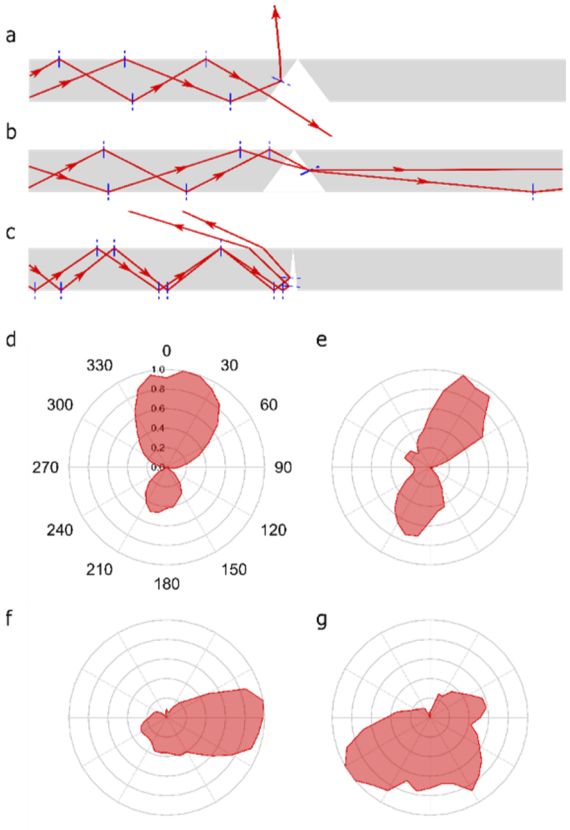


**Fig. 3.** (a-c) Simulation model illustrating light behaviour at the micro-window depending upon the light incident angle and the geometry of the micro-window. (d-g) Radar plots showing the normalised power distribution around the circumference of the fibre (Fibre A) for 4 micro-windows. The absolute location of the micro-window is set at 0 degrees.

Figures 3(d)–3(g) are radar plots of the radial power distribution measured around 4 machined emission windows. The location of the micro-window in the POF was found using a lensed CCD camera imaging system mounted on the rotational mount (at the same position as PD1 in Fig. 2(a)). As shown, the distribution of light varies largely across the micro-windows, which is an artefact of the structural geometry of the micro-windows. For smooth angled micro-window surfaces, one might expect a well-defined unidirectional emission profile. Compared to glass optical fibres, where the geometry of the micro-window can be precisely controlled by adjusting the laser power [20], the structural properties of the PMMA fibre results in a window with a complex surface profile. As seen in Figs. 3(d)–3(g), while emission is sometimes aligned to or opposite the machined window, this is not always the case. Particularly Fig. 3(f) shows an example of emission at 90 degrees to the window, due to a complex machined profile. It is noted this emission profile is highly dependent on the proximal coupling, as discussed further. The surface morphology of the micro-windows might be significantly changed by ultrasonic etching techniques [30] which are known to result in a cleaner and smoother micro-window. This will be investigated for future applications.

Optics EXPRESS

Cross coupling of light in the POF cores was also quantified. For this, 780 nm light from an SMF was coupled into a single core in the middle of the cross section of a 1.5 m long fibre. The light distribution at the distal end of the POF was imaged using a CCD camera and the amount of light in each core quantified. It is observed that ~20% of the light from the excited core is coupled to adjacent cores through evanescent coupling and that the cross-coupling of light between the cores varies by ± 3% across the fibre. The spatial properties of the light emitted from the micro-windows will also include contributions from the light contained in the evanescently excited cores, increasing complexity of emission.

#### 2.2.3. Micro-window full emission profile

So far, the radar plot provides information on the intensity distribution at a specific position along the fibre axis relative to the micro-windows. As observed in the simulation model, forward or reverse emission angles are also expected to be dependent on the noted complex micro-window geometry. Here a new technique is needed to record a fuller profile across as much of the light emission sphere as possible. To investigate this overall side-firing intensity distribution at the micro-windows, further measurements were carried out in which the PD1 in Fig. 2(a) is replaced with a lensed camera system (DCC1545M-GL) which can be rotated 360 degrees (°) around the fibre axis. We used a table tennis "ping-pong" ball as a semi-transparent screen onto which the light emitted from the micro-window could be projected. To do so, the ball (diameter 40 mm) was placed inside a 2-inch aperture beamspliter cube and the fibre was fed through two holes drilled on either side of the ball. The diameter of the ball was measured using digital vernier callipers as a calibration and the position of the micro-window was set at the centre of the ball. Emission from the micro-window was optimised and images of the ping-pong ball were taken at different angles around the fibre axis.

Figure 4(a) presents the side images of the ball which are normalised to the maximum pixel value in the entire row (dotted blue box). We also observed that the emission profile from a micro-window can be changed significantly by changing the input coupling conditions. Figures 4(b)–4(d) presents the emission profiles for three other input coupling conditions. A second lensed camera system (DCC1545M-GL) was used to image the light distribution on the surface of the ping-pong ball when viewed along the fibre optical axis, black dotted box in Fig. 4 (normalised to the maximum pixel count among the two images). The two images were taken at equal distances from the front and back ends of the ball. Due to the 1-inch aperture of the optomechanical mounts, only a portion of the ping-pong ball in the centre is captured (23.6 mm) for the front and back images. The amount of light measured at the distal end of the fibre using PM2 (Fig. 2(a)) differed by ± 5% to the mean for the four coupling conditions, indicating that the coupling efficiency to the fibre itself was minimally affected. This confirms our ability to control, to some degree, the emission profile of the light exiting the side of the fibre. As the laser modification ablates a group of cores, we can thus excite multiple cores at the proximal end of the POF to obtain a range of emission profiles, which may be relevant for future applications.

#### 2.2.4. Characterisation of side-coupling efficiency

To properly quantify the fraction of input light side-emitted, back-scattered and forward-scattered from each micro-window we performed a series of cut-back measurements. Initially, light was launched into the POF (Fibre A) in such a way as to roughly maximise the side emission from the $12^{th}$ micro-window (furthest from the input). The end-facet of the fibre, 1 cm away from the micro-window was then placed inside an integrating sphere (IS) (Thorlabs S142C detector). A small piece of highly absorbing black sticky tape was placed on the end of the fibre to absorb the forward propagating light. With the micro-window inside the active area of the IS, the side-emitting power was further optimised by tuning the input coupling. For this coupling condition, a maximum power value was measured by the IS (measurement 1, M1).

Optics EXPRESS

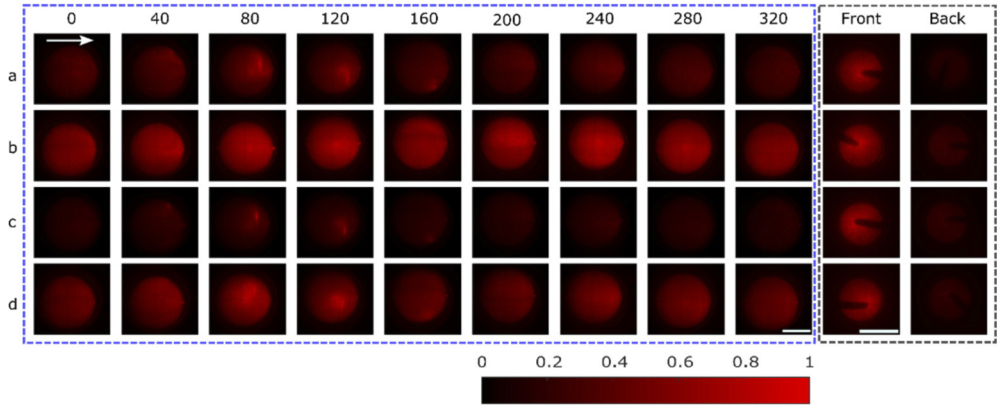


**Fig. 4.** (a-d) (blue dotted box) Normalised emission profiles from a micro-window for 4 different input coupling conditions. The white arrow in the top left indicates the light propagation direction. The title in each column represents the angle of the camera relative to the micro-window for side imaging. The location of the micro-window is set centrally facing out of the page (0°) for a-d. Scale bar: 20 mm. (black dotted box) The front and back images were taken with a different camera and separately normalised. Scale bar: 20 mm. See the animation Visualization 2 of the different side image intensity distributions in one coupling condition.

The black tape was then removed, and the power was re-measured. This power measurement (measurement 2, M2) contains contributions from the side emission and the forward scattered light. Lastly, the POF was cut directly before (towards the launch end of the fibre) the location of the micro-window and the total guided power measured again with the IS (measurement 3, M3). M1, M2 and M3 are measured separately for each emission window as an independent cutback measurement. By comparing the three power values measured the fraction of light side-emitted can be estimated as M1/M3, the fraction of light back-scattered can be estimated as (M3-M2)/M3 and the fraction of forward-scattered light can be estimated as (M2-M1)/M3.

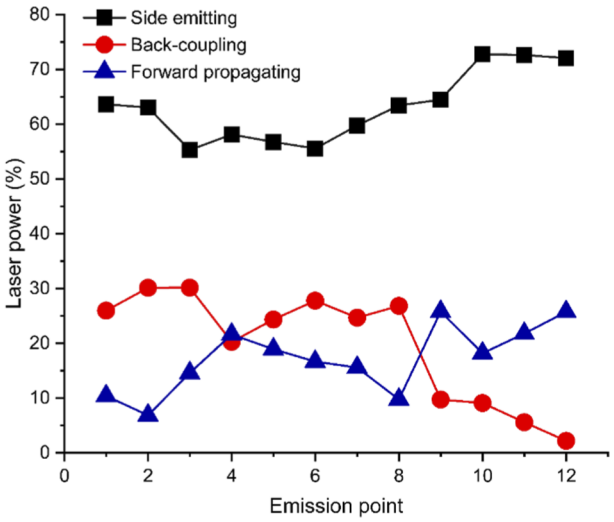


**Fig. 5.** Emission characterisation of the micro-windows measured using a cutback technique.

Optics EXPRESS

These cutback measurements were repeated for each micro-window and are presented in Fig. 5. To reduce measurement errors, for each cutback the fibre facet was hand polished to avoid optical loss due to defects and imperfections at the facet arising from a bad cleave. The measured throughputs of the machined micro-windows were found to range from 55% to 73% across the 12 micro-windows. By comparing the power of light just after the coupling fibre (SM600 Fig. 2(a)), the input coupling loss in our throughput measurement was found to be 0.22 dB.

## 3. Conclusion and future applications

This paper presents the fabrication of high throughput, multipoint light-emitting fibres using femtosecond laser micro-ablation. We observed that by ablating multiple cores in selected regions of a polymer MCF, 3D light delivery and illumination at desired locations can be obtained with ability to control the light emission profile and output direction.

Key novelty is the creation of limited micro-windows affecting subsets of the large number of total cores, this allowing the choice of which single light emission location is illuminated by controlling proximal coupling. The movie Visualization 1 demonstrates this with serial automated illumination of 91 emission points in Fibre B. As such, emission points can be considered independently. Complex emission profiles are observed – studied both radially around the fibre axis and on a ping-pong ball screen to observe a fuller profile. The ability to tune this emission profile through proximal coupling adjustment (with only 5% variation in light throughput) offers intriguing possibilities for applications benefiting from deliberately controllable emission directionality. However, it is also noted the complex profile of the micro-windows does not at this time lead to a predictable response.

It would also be possible to illuminate all emission locations simultaneously if desired. Flood illumination of the proximal fibre facet would achieve this, but at notable loss of throughput efficiency as the central cores would not contribute to emission. However, if annulus illumination were used higher efficiency could be recovered. In combination with careful optimisation of micro-window radial location to fill the annulus, it is imaginable to recover the intrinsic throughput of the emission points, measured to be in the range 55% to 73% with a fibre cut back method. Thus, the core technology developed here may offer both selected single point emission, or simultaneous many point emission, as required by the application.

It is possible to imagine many potential photonic applications, we consider in more detail how this fibre technology can benefit a few spanning biomedical sensing, imaging, and therapy. In photobiomodulation [5] or photodynamic therapy (PDT) [31] applications, delivering light to specific areas of tissues or organs for photophysical and photochemical effect is an essential criterion. However, guidance of in-vivo instrument insertion can be challenging. This technology would offer the possibility of fibre placement internally and post-selection of the illumination region. While results presented here demonstrate 1 cm separation between illumination points, closer separation would be easily achieved for finer control. As such specific organ regions could be illuminated, with >55% throughput offering efficient delivery of therapeutic light.

Discrete light emission (and therefore collection) provided by these fibres is also potentially enabling in medical diagnostics in the form of spectroscopic investigation at multiple points along a medical device throughout an organ or extended tissue structure. In the case of therapeutic treatment (photobiomodulation [5] or photodynamic therapy [31]) this offers determination of which emission locations should be subsequently used for treatment, for instance observing where the PDT agent has accumulated in tumours through its fluorescent properties ([31]). Thus, the selectivity of the light emission/collection location demonstrated here removes the need for precise instrument placement.

Potential applications exist for superficial indwelling medical device insertion, such as catheter placement, light emission along the length of the catheter could be viewed through the skin.

Optics EXPRESS

Again, it would be possible to only illuminate the relevant fibre locations, concentrating delivered illumination power levels safe in a medical environment only where beneficial.

For device placement deeper in tissue, in which light must transit through significant portions of highly scattering biological media, the discrete sources of light may act as known points which can be located serially. Here user selective emission from a single micro-window structures with > 55% throughput delivers the single bright guide point required. In particular, we can sequentially illuminate the machined point sources along the fibre length with short pulse laser light and use time-resolved techniques to observe the transport of light emitted from these discrete locations. Using 2D time-resolved imaging cameras, NIR light scattered deep from the tissue can be monitored and used for time-domain diffuse spectroscopy [32], optical tomography [33], and medical device location [34]. By creating light emission at desired points, we anticipate that it may be possible to determine the full path of an inserted optical fibre device.

The ability to select individual fibre emission points can be enabled with beam-steering optomechanics to couple light into specific cores, providing the rapid and repeatable illumination at discrete locations enabling many applications as described. Such techniques could potentially replace or enhance current clinical illumination methods based on diffusive fibre tips to deliver light to complex tissue structures with greater control.

**Funding.** Engineering and Physical Sciences Research Council (EP/K03197X/1, EP/R005257/1); Science and Technology Facilities Council (ST/S000658/1, ST/S000763/1).

**Disclosures.** The authors declare no conflicts of interest.

**Data availability.** Data underlying the results presented in this paper are available in Ref. [35].

## References

1. S. A. Costello, J. Nyikal, V. Y. H. Yu, and P. McCloud, "BiliBlanket phototherapy system versus conventional phototherapy: A randomized controlled trial in preterm infants," J. Paediatr. Child Health **31**(1), 11–13 (1995).
2. J. Spigulis, D. Pfafrods, and M. Stafeckis, "Optical fiber diffusive tip designs for medical laser-lightguide delivery systems," Proc. SPIE **2328**, 69–75 (1994).
3. E. G. Rawson, "Analysis of Scattering from Fiber Waveguides with Irregular Core Surfaces," Appl. Opt. **13**(10), 2370–2377 (1974).
4. A. Arie, R. Karoubi, Y. S. Gur, and M. Tur, "Measurement and analysis of light transmission through a modified cladding optical fiber with applications to sensors," Appl. Opt. **25**(11), 1754–1758 (1986).
5. R. Zomorrodi, G. Loheswaran, A. Pushparaj, and L. Lim, "Pulsed Near Infrared Transcranial and Intranasal Photobiomodulation Significantly Modulates Neural Oscillations: a pilot exploratory study," Sci. Rep. **9**(1), 6309 (2019).
6. L. Wondraczek, A. Gründler, A. Reupert, K. Wondraczek, M. A. Schmidt, G. Pohnert, and S. Nolte, "Biomimetic light dilution using side-emitting optical fiber for enhancing the productivity of microalgae reactors," Sci. Rep. **9**(1), 9600 (2019).
7. I. Peshko, V. Rubtsov, L. Vesselov, G. Sigal, and H. Laks, "Fiber photo-catheters for invasive and less invasive treatment of atrial fibrillation," Proc. SPIE **5969**, 59691W (2005).
8. R. George and L. J. Walsh, "Performance assessment of novel side firing flexible optical fibers for dental applications," Lasers Surg. Med. **41**(3), 214–221 (2009).
9. A. J. Conneely, C. Bennett, G. M. O'Connor, T. Vollmerhausen, C. O'Byrne, G. Spence, D. Rowe, and J. Victor, "Generation of side-emitting polymer optical fibres by laser ablation for use in antimicrobial applications," in *35th International Congress on Applications of Lasers & Electro-Optics (ICALEO) (2016)*,M604 (2016).
10. A. N. Zorzos, E. S. Boyden, and C. G. Fonstad, "Multiwaveguide implantable probe for light delivery to sets of distributed brain targets," Opt. Lett. **35**(24), 4133–4135 (2010).
11. I.-B. Sohn, Y. Kim, Y.-C. Noh, I. Won Lee, J. K. Kim, and H. Lee, "Femtosecond laser and arc discharge induced microstructuring on optical fiber tip for the multidirectional firing," Opt. Express **18**(19), 19755–19760 (2010).
12. G. Wang, C. Wang, Z. Yan, and L. Zhang, "Highly efficient spectrally encoded imaging using a 45° tilted fiber grating," Opt. Lett. **41**(11), 2398–2401 (2016).
13. S. H. Lee, Y.-T. Ryu, D. H. Son, S. Jeong, Y. Kim, S. Ju, B. H. Kim, and W.-T. Han, "Radial-firing optical fiber tip containing conical-shaped air-pocket for biomedical applications," Opt. Express **23**(16), 21254–21263 (2015).
14. O. Shapira, K. Kuriki, N. D. Orf, A. F. Abouraddy, G. Benoit, J. F. Viens, A. Rodriguez, M. Ibanescu, J. D. Joannopoulos, Y. Fink, and M. M. Brewster, "Surface-emitting fiber lasers," Opt. Express **14**(9), 3929–3935 (2006).
15. C. Kim, H. Park, and H. Lee, "Comparison of laser-induced damage with forward-firing and diffusing optical fiber during laser-assisted lipoplasty," Lasers Surg. Med. **45**(7), 437–449 (2013).
16. A. Reupert, M. Heck, S. Nolte, and L. Wondraczek, "Side-emission properties of femtosecond laser induced scattering centers in optical fibers," Opt. Mater. Express **9**(6), 2497–2510 (2019).

Optics EXPRESS


17. R. R. Gattass and E. Mazur, "Femtosecond laser micromachining in transparent materials," Nat. Photonics **2**(4), 219–225 (2008).
18. H. Nguyen, M. M. Parvez Arnob, A. T. Becker, J. C. Wolfe, M. K. Hogan, P. J. Horner, and W.-C. Shih, "Fabrication of multipoint side-firing optical fiber by laser micro-ablation," Opt. Lett. **42**(9), 1808–1811 (2017).
19. C. B. Schaffer, A. Brodeur, J. F. García, and E. Mazur, "Micromachining bulk glass by use of femtosecond laser pulses with nanojoule energy," Opt. Lett. **26**(2), 93–95 (2001).
20. L. Athanasekos, M. Vasileiadis, A. El Sachat, N. A. Vainos, and C. Riziotis, "ArF excimer laser microprocessing of polymer optical fibers for photonic sensor applications," J. Opt. **17**(1), 015402 (2015).
21. I. B. Sohn, Y. Kim, Y. C. Noh, J. C. Ryu, and J. T. Kim, "Microstructuring of optical fibers using a femtosecond laser," J. Opt. Soc. Korea **13**(1), 33–36 (2009).
22. R. Irawan, T. S. Chuan, T. C. Meng, and T. K. Ming, "Rapid Constructions of Microstructures for Optical Fiber Sensors Using a Commercial CO2 Laser System," Open Biomed. Eng. J. **2**(1), 28–35 (2008).
23. B. N. Chichkov, C. Momma, S. Nolte, F. Von Alvensleben, and A. Tünnermann, "Femtosecond, picosecond and nanosecond laser ablation of solids," Appl. Phys. A **63**(2), 109–115 (1996).
24. C. B. Schaffer, A. Brodeur, and E. Mazur, "Laser-induced breakdown and damage in bulk transparent materials induced by tightly focused femtosecond laser pulses," Meas. Sci. Technol. **12**(11), 1784–1794 (2001).
25. K. Itoh, W. Watanabe, S. Nolte, and C. B. Schaffer, "Ultrafast processes for bulk modification of transparent materials," MRS Bull. **31**(8), 620–625 (2006).
26. T. Kaino, "Absorption losses of low loss plastic optical fibers," Jpn. J. Appl. Phys. **24**(Part 1, No. 12), 1661–1665 (1985).
27. J. Zubia and J. Arrue, "Plastic optical fibers: An introduction to their technological processes and applications," Opt. Fiber Technol. **7**(2), 101–140 (2001).
28. J. Militky, D. Kremenakova, and J. Saskova, "Optical Attenuation of Linear Composites Containing SEPOF," in *IOP Conference Series: Materials Science and Engineering 460* (2018), p. 012035.
29. A. T. Becker and H. Nguyen, "Defects in an optical fiber," Wolfram Demonstrations Project, Oct. 2016, https://demonstrations.wolfram.com/DefectsInAnOpticalFiber.
30. M. Zhao, L. Dai, N. Zhong, Z. Wang, M. Chen, B. Li, B. Luo, B. Tang, S. Shi, T. Song, and X. Zou, "Wet etching technique for fabrication of a high-quality plastic optical fiber sensor," Appl. Opt. **56**(31), 8845–8850 (2017).
31. S. Benson, F. de Moliner, A. Fernandez, E. Kuru, N. L. Asiimwe, J. S. Lee, L. Hamilton, D. Sieger, I. R. Bravo, A. M. Elliot, Y. Feng, and M. Vendrell, "Photoactivatable metabolic warheads enable precise and safe ablation of target cells in vivo," Nat. Commun. **12**(1), 2369 (2021).
32. S. Mosca, P. Lanka, N. Stone, S. Konugolu Venkata Sekar, P. Matousek, G. Valentini, and A. Pifferi, "Optical characterization of porcine tissues from various organs in the 650–1100 nm range using time-domain diffuse spectroscopy," Biomed. Opt. Express **11**(3), 1697–1706 (2020).
33. M. Alayed and M. J. Deen, "Time-resolved diffuse optical spectroscopy and imaging using solid-state detectors: Characteristics, present status, and research challenges," Sensors **17**(9), 2115 (2017).
34. M. G. Tanner, T. R. Choudhary, T. H. Craven, B. Mills, M. Bradley, R. K. Henderson, K. Dhaliwal, and R. R. Thomson, "Ballistic and snake photon imaging for locating optical endomicroscopy fibres," Biomed. Opt. Express **8**(9), 4077–4095 (2017).
35. H. K. Chandrasekharan, "Ultrafast laser ablation of a multicore polymer optical fibre for multipoint light emission," Heriot-Watt University (2021), https://doi.org/10.17861/dd4ad1f9-ce71-4ba4-93dc-0a22fa639fca